Derlin-2 deficient mouse reveals an essential role for protein dislocation in chondrocytes

Stephanie K. Dougan[1], Chih-Chi Andrew Hu[1*], Marie-Eve Paquet[1,6*], Matthew B. Greenblatt[2], Jun Kim[3], Brendan N. Lilley[4], Nicki Watson[1], Hidde L. Ploegh[1,7]

1. Whitehead Institute for Biomedical Research, 9 Cambridge Center, Cambridge, MA 02142, USA.

2. Department of Immunology and Infectious Diseases, Harvard School of Public Health, Boston, MA 02115, USA

3. Massachusetts Institute of Technology, Cambridge, MA 02139

4. Department of Molecular and Cellular Biology and Center for Brain Science, Harvard University, Cambridge, MA 02138, USA

5. Department of Medicine, Harvard Medical School, Boston, MA 02115, USA

6. Current address: Centre de recherche Université Laval Robert-Giffard, 2601 Chemin de la Canardière F6500, Québec, QC

7. To whom correspondence should be addressed, ploegh@wi.mit.edu.

*, These authors contributed equally to this work.

Contact: Hidde Ploegh
Whitehead Institute for Biomedical Research
9 Cambridge Center, Rm 361
Cambridge, MA 02142
phone (617) 324-2031
fax (617) 452-3566
ploegh@wi.mit.edu

Conflict of Interest Statement: The authors declare no conflict of interest.

Abstract

Protein quality control is a balance between chaperone-assisted folding and removal of misfolded proteins from the ER. Cell-based assays have been used to identify key players of the dislocation machinery, including members of the Derlin family. We generated a conditional knockout mouse to examine the in vivo role of Derlin-2, a component that nucleates cellular dislocation machinery. In most Derlin-2 deficient tissues, we found constitutive upregulation of ER chaperones and IRE-1 mediated induction of the unfolded protein response. The IRE-1/XBP-1 pathway is required for development of highly secretory cells, particularly plasma cells and hepatocytes. However, B lymphocyte development and antibody secretion were normal in the absence of Derlin-2. Likewise, hepatocyte function was unaffected by liver-specific deletion of Derlin-2. Whole body deletion of Derlin-2 results in perinatal death. The few mice that survive to adulthood all developed skeletal dysplasia, likely caused by defects in collagen matrix protein secretion by costal chondrocytes.

Introduction

Protein quality control is important: accumulation of misfolded proteins can cause a variety of diseases such as cystic fibrosis, Alzheimer's disease, and spinocerebellar ataxia (1). Protein quality control occurs in all subcellular compartments where misfolded proteins arise or accumulate (cytosol, ER, lysosomes, etc.). In the example of cystic fibrosis, CFTR, a protein critical for chloride transport, is inactivated by mutations that impair its proper folding. In other cases, accumulation of mutant protein into amyloid aggregates causes disease. Amyloid-induced toxicities are common causes of neurodegenerative diseases such as Parkinson's, Alzheimer's and Huntington's disease. For each of the known protein quality control diseases, a specific misfolded protein has been identified as the causative agent (1). One might therefore assume that more global defects in protein folding would also lead to pathologies, yet this hypothesis has been difficult to test.

Protein quality control in the ER is achieved through chaperone-assisted folding and by removal of terminally misfolded proteins for destruction via the ubiquitin-proteasome system (2, 3). Folding status is monitored by a large variety of chaperones, and folding itself is regulated by chaperones as well. Misfolded glycoproteins may be recognized by calnexin and calreticulin which bind to monoglucosylated N-linked glycans. Protein disulphide isomerase (PDI) catalyzes the oxidation and reduction of disulphide bonds and also recognizes non-native structures. The importance of chaperones in the ER is underscored by the fact that genetic loss of most ER chaperones causes embryonic lethality (3).

If proteins that enter the ER fail to fold properly, they must be removed from the ER, often in a process called dislocation (2). How misfolded proteins are recognized is not completely understood. Proteins with N-linked glycans may be recognized by members of the EDEM protein family which enhance dislocation of certain misfolded proteins (4). The lectin domain-containing OS-9 protein also binds to alternate mannose-containing isomers, as well as to some misfolded proteins that lack N-linked glycans. OS-9 interacts directly with HRD-1 and Sel1L, a ubiquitin ligase complex that interacts with

Derlin 1 and Derlin 2 (5, 6). The Derlin family proteins contain four transmembrane domains and are thought to oligomerize in the ER lipid bilayer and may contribute to the formation of a dislocation pore (7-9). Misfolded proteins are extracted through the action of the cytosolic p97 AAA-ATPase which binds to the Derlins through the adaptor protein VIMP (8, 10). Attachment of at least one ubiquitin moiety is required for recognition by p97, although the ubiquitin is removed prior to full extraction from the ER (8, 10). Several E3 ubiquitin ligases and deubiquitinating (DUBs) enzymes have been implicated in dislocation of misfolded proteins; among these are Ubc6e and YOD1 (5, 11).

Cells respond to misfolded proteins via three arms of the unfolded protein response (UPR) (12). PERK, ATF6 and IRE-1 are transmembrane proteins that reside in the ER, functionally coupled to ER quality control machinery. Accumulation of misfolded proteins in the ER can trigger each of these three UPR sensors by as yet poorly defined mechanisms. Activation of PERK results in phosphorylation of eIF2α, which causes attenuation of protein synthesis (13). Paradoxically, the ATF4 mRNA, which encodes a transcription factor, is translated better under these circumstances. Increased ATF4 levels lead to transcriptional activation of several ER chaperones, genes involved in amino acid metabolism and transport, and CHOP (14). The second UPR sensor, ATF6, is found in the ER and interacts with BiP through its luminal domain. Dissociation from BiP exposes a Golgi localization sequence in ATF6, and once in the Golgi, ATF6 is cleaved by site-1 and site-2 proteases to release the 50 kDa active form of the ATF6 transcription factor, which then translocates to the nucleus (15). ATF6 activates transcription of BiP, XBP-1, various components of ER quality control and CHOP. IRE-1, evolutionarily the most ancient of the ER stress sensors, is activated upon dimerization and autophosphorylation (16, 17). The cytoplasmic domain of IRE-1 catalyzes an unconventional RNA splicing event to remove a short sequence from XBP-1 mRNA (18). The resulting spliced XBP-1 protein (XBP-1s) translocates to the nucleus and activates transcription of ER chaperones and enzymes involved in lipid biosynthesis to allow expansion of the ER (19).

Knockout mice exist for all three arms of the UPR. *Perk*$^{-/-}$ mice are born at Mendelian ratios, but show defects in both the endocrine and exocrine pancreas. They develop overt diabetes by 4 weeks of age (20). Accumulation of misfolded proteins can be observed directly in *Perk*$^{-/-}$ pancreatic islet and acinar cells by electron microscopy, which shows distended, electron dense ER structures (20). Two *Atf6* genes, *Atf6*α and *Atf6*β are present in mammals, and these have some functional redundancy. *Atf6*$\alpha^{-/-}$ mice are phenotypically normal, but develop liver steatosis upon intraperitoneal challenge with tunicamycin (21). The combined *Atf6*α/β double knockout is lethal at a stage prior to embryonic day 8.5, possibly due to an inability to transcribe genes that encode critical ER chaperones such as BiP (22). Indeed, *Bip*$^{-/-}$ mice also die at an early stage of embryonic development (23). Both *Ire-1*$\alpha^{-/-}$ and *Xbp1*$^{-/-}$ mice die around embryonic day 13.5 due to liver failure (24). IRE-1β is expressed primarily in intestinal epithelial cells, and deletion of *Ire1*β renders mice susceptible to sodium dextran sulphate-mediated colitis (25). Conditional ablation of *Xbp1* in B cells or in intestinal epithelial cells uncovered an essential requirement for XBP-1 in formation of plasma cells and Paneth cells, respectively (26, 27). Although XBP-1 induction in B cells occurs independently of unfolded protein accumulation, XBP-1 plays an important role in plasma cell formation through modulation of lipid synthesis, regulation of transcription factor expression and homing of plasma cells to the bone marrow (28, 29).

Blocking any of the three arms of the unfolded protein response should lead to an increase in misfolded proteins in tissues that are likely to experience ER stress because of a high secretory load. Loss of PERK, ATF6 and IRE-1 pathways primarily affects organs such as the liver and pancreas, as well as specific secretory cell types such as B cells and Paneth cells. Although all arms of the UPR cause upregulation of BiP and other ER chaperones, the majority of transcriptional targets for ATF4, ATF6 and XBP-1s are non-overlapping (30, 31). Furthermore, different tissues rely on the different UPR components to different extents. As a consequence, *Perk*$^{-/-}$, *Atf6*$^{-/-}$ and *Ire1*$^{-/-}$ mice have quite different phenotypes. In general, however, disruption of any single branch of the UPR has serious adverse consequences.

Here we report a knockout mouse model of a protein involved in ER dislocation. Derlin-2 interacts with Derlin-1, Sel1L, VIMP, p97, HRD-1, OS-9 and Ubc6e to form a dislocation complex involved in the removal of misfolded substrates from the ER (5, 6, 8). Derlin-2 appears to be more abundant and is present at a higher level than Derlin-1 in the Sel1L-nucleated dislocation complex. Silencing of Derlin-2 impairs dislocation of the Null Hong Kong version of α1-antitrypsin (32). We show that the Derlin-2 deficient mouse displays constitutive activation of the UPR, and we demonstrate further an unexpected role for Derlin-2 in cartilage formation.

Results

Derlin-2 conditional knockout mouse confirms a role for Derlin-2 in ER dislocation.

To study the role of Derlin-2 in different tissues, we generated a conditional knockout mouse in which the Derlin-2 gene is flanked by loxp sites (Supplemental Figure 1). The resulting Derlin-2 flox/flox mouse was crossed to mice expressing cre recombinase driven by the CMV promoter, by the CD19 promoter or by the albumin promoter. The resulting *Der2*$^{-/-}$, *Der2*^{CD19} and *Der2*^{Alb} mice have Derlin-2 deleted in all tissues, in B cells or in hepatocytes, respectively.

Previous work implicating the Derlins in removal of misfolded proteins from the ER has relied on RNA silencing or overexpression of dominant negative Derlin proteins (7-9). To show by genetic means that Derlin-2 is involved in ER dislocation, we generated mouse embryonic fibroblasts (MEFs) from embryonic day 13.5 Derlin-2 deficient fetuses or their wildtype littermates. *Der2*$^{-/-}$ MEFs were then transfected with plasmids expressing ribophorin fragment (RI332) or the Null Hong Kong variant of α1-antitrypsin (NHK). Both RI332 and NHK failed to be dislocated at normal rates in *Der2*$^{-/-}$ MEFs, as shown by ER retention during pulse chase analysis (Figures 1A and 1B). On the other hand, we found no evidence for a systemic defect in the secretory pathway, since properly folded secretory or membrane proteins traverse the ER normally, as shown by equivalent secretion of wild type α1-antitrypsin and equal maturation of class I MHC (Figures 1B and 1C).

Der2 -/- MEFs upregulate members of the dislocation complex and have a constitutive UPR.

Lysates from two independent wild type MEF lines (lanes 1, 2) and four independent *Der2*$^{-/-}$MEF lines (lanes 3-6) were immunoblotted for various ER resident proteins and proteins involved in the UPR (Figure 2A). Sel1L, HRD-1, OS-9 and Ubc6e, all members of the Derlin dislocation complex, were upregulated in *Der2*$^{-/-}$MEFs. This compensatory upregulation did not apply to Derlin-1; Derlin-1 protein levels were decreased in the absence of Derlin-2 despite increased levels of Derlin-1 transcripts (Figure

2A and data not shown), suggesting that the loss of Derlin-2 destabilizes Derlin-1 but not other known components of the dislocation complex.

IRE-1α, XBP-1s, BiP and GRP94 were upregulated in *Der2*$^{-/-}$MEFs, indicating induction of the UPR (Figure 2A). Although the UPR can proceed through three pathways in eukaryotes, the IRE-1 axis seemed to be the only pathway induced in *Der2*$^{-/-}$MEFs. ATF-6 was not increased (data not shown), and elongation factor 2-α (eIF2α) phosphorylation was not increased, suggesting that the PERK pathway for UPR induction was not induced by the absence of Derlin-2.

MEF lysates were compared in a side-by-side analysis with lysates from naïve B cells, liver and chondrocytes (derived from wild type or *Der2*^{CD19}, *Der2*^{Alb} or *Der2*$^{-/-}$, respectively). In all tissues analyzed, Derlin-1 protein levels were decreased in Derlin-2 deficient cells (Figure 2B). OS-9 and Sel1L were strongly upregulated in *Der2*$^{-/-}$ MEFs and chondrocytes, but were affected to a lesser degree in B cells and liver, underscoring the cell and tissue type-specific aspects of the UPR (Figure 2B).

Loss of Derlin-2 in B lymphocytes has no effect on B cell development or antibody secretion.

Der2^{CD19} mice were born at normal Mendelian ratios as expected (data not shown). We were particularly interested in the B cell compartment, because IRE-1 deficiency affects B cell development (33). B cell subset analysis showed no defects in the percentage or total number of follicular, marginal zone, B-1, transitional T1 or T2, germinal center B cells or plasma cells (Figure 3A and Supplemental Table 1) in *Der2*^{CD19} mice: developing B cells in the bone marrow showed normal percentages of pro, pre and immature B cell populations (Supplemental Table 1).

Upon antigen engagement, naïve B cells develop into antibody-secreting cells and eventually into long-lived plasma cells which continue to secrete antibodies for the remainder of the organism's life. The early stages of this process can be replicated in vitro by addition of lipopolysaccharide (LPS), which converts naïve B cells into antibody-secreting B cell blasts. The high rates of immunoglobulin secretion place extreme demands on the functional capacity of the ER. We therefore chose this model as a likely

cell type that might reveal even slight perturbations in quality control in the secretory pathway, as has been demonstrated for α1-antitrypsin in fibroblasts. However, metabolic labeling of *Der2*^{CD19} LPS blasts showed no defects in the rates of antibody production or secretion (Figures 3B and 3C).

Consistent with the apparent lack of effect of Derlin-2 in B cell development and function, immunoblotting of B cell lysates at various stages of LPS stimulation showed little differences in ER chaperones or dislocation complex members (Figure 3D), with the exception of Derlin-1, which showed a decrease similar to that seen in MEFs (Figure 2A and 2B). Neither IRE-1α nor XBP-1 protein levels were increased in Der2CD19 LPS blasts. Loss of Derlin-2 does not obviously enhance UPR activation in developing B cell blasts. By comparison, XBP-1 deficient LPS blasts, which are known to have defects in antibody secretion, show strong upregulation of IRE-1α (Figure 3D) (28).

Loss of Derlin-2 in hepatocytes has negligible effect on liver function despite an ongoing UPR.

Der2^{Alb} mice were also born at normal Mendelian ratios (data not shown). No differences were found in serum glucose or serum triglycerides in either fasting (Figures 4A and 4B) or fed mice (data not shown). *Atf6α*$^{-/-}$ and *Chop*$^{-/-}$ mice show mild phenotypes at baseline, but rapidly succumb to severe liver or kidney disease when challenged with moderate amounts of tunicamycin to induce the unfolded protein response (21, 34). *Der2*^{Alb} mice and their wild type littermates were injected intraperitoneally with tunicamycin and sacrificed when their body weights reached 80% of baseline. *Der2*^{Alb} mice succumbed at the same rate as control mice (Figure 4C). Hepatocytes secrete the majority of serum proteins. We therefore assayed various serum protein levels as a measure of liver secretory function. *Der2*^{Alb} mice showed no signs of anemia (spun hematocrit levels: *Der2*^{Alb} = 48.2 +/- 2.0; littermate controls = 46.0 +/- 2.0) and had normal levels of serum transferrin (Figure 4D). The levels of α1-antitrypsin were likewise unaffected (Figure 4D) and a functional assay for inhibition of elastase activity showed no difference (Figure 4E) between wild type and *Der2*^{Alb} mice. Total serum albumin was also comparable between *Der2*^{Alb} and control mice (data not shown).

Hepatocyte function is tightly linked to nutrient status; thus hepatocyte lysates were prepared from mice that had been fasted for 24 hours and mice that had been fed ad libitum (Figure 4F). Under starvation conditions, normal hepatocytes express less Derlin-2 protein (Figure 4F). As in MEFs, members of the Derlin dislocation complex Sel1L, HRD-1 and Ubc6e showed compensatory upregulation in the absence of Derlin-2. OS-9, which was upregulated more than 10-fold in MEFs, was unaffected in Derlin-2 deficient hepatocytes. Different tissues must therefore adapt to loss of Derlin-2 in different ways (Figures 2B and 4G). *Der2*^{Alb} hepatocytes showed increases in IRE-1α and XBP-1s, both of which were somewhat attenuated by starvation. Thus, hepatocytes in *Der2*^{Alb} mice have an ongoing UPR, which is modified only slightly by the nutrient status of the mice (Figure 4F).

Hepatocytes were isolated from *Der2*^{Alb} mice or their wild type littermates and cultured ex vivo on collagen-coated plates. Metabolic labeling of these primary hepatocyte cultures showed no obvious differences in the profiles of intracellular (Figure 5A) or secreted proteins (Figure 5B). Apolipoprotein B is one of the largest proteins synthesized by hepatocytes and is regulated not only by stop transfer sequences that induce ribosome pausing, but also by p97-mediated ER dislocation (35, 36). Pulse chase analysis of apolipoprotein B (apoB-48) showed no differences in the rate of synthesis or secretion of apoB-48 particles or their associated albumin (Figures 5C and 5D).

Whole body deletion of Derlin-2 leads to perinatal lethality and skeletal abnormalities.

To achieve complete deletion of Derlin-2, we crossed Derlin-2 flox/flox mice to mice transgenic for Cre driven by the CMV promoter. After one generation, the resulting mice were heterozygous for one deleted Derlin-2 allele and one wild type Derlin-2 allele. These mice were then intercrossed and should have yielded Derlin-2 deleted/deleted pups at 25% frequency. However, *Der2*$^{-/-}$ mice represented only 4% of mice at weaning (n = 160). Genotyping of embryos at embryonic day 17.5-18.5 showed normal Mendalian inheritance, and no obvious abnormalities were observed in the *Der2*$^{-/-}$ embryos. Closer inspection of *Der2*$^{-/-}$ containing litters revealed several dead or dying pups 24 hours after birth, and

genotyping of 1 day old mice with inclusion of the dead or dying pups showed *Der2*$^{-/-}$ mice to be 23.7% of the total. Thus, *Der2*$^{-/-}$ pups are born at Mendelian ratios, but the majority dies within 24 hours of birth.

To determine the cause of death, several litters containing *Der2*$^{-/-}$ pups were delivered by caesarean section. All pups breathed normally and were not cyanotic, suggesting that lung abnormalities and neural innervation of the diaphragm were not causes of death. Histological analysis of one-day old *Der2*$^{-/-}$ pups showed no obvious cause of death, and serial sections of the heart showed no abnormalities (data not shown). The gross structures of the central and peripheral nervous systems and the formation of neuromuscular synapse formation were examined in *Der2*$^{-/-}$ pups and found to be normal (Supplemental Figure 2). All neonatal mice are hypoglycemic; *Der2*$^{-/-}$ mice that had been delivered via caesarean section and deprived of food showed no evidence of increased hypoglycemia at two hours post-birth (Figure 6A). *Der2*$^{-/-}$ mice that were delivered vaginally and left with their mothers refused to feed. *Der2*$^{-/-}$ pups consistently lacked milkspots and later died of starvation (Figure 6B). Hand-feeding of *Der2*$^{-/-}$ pups showed that milk could reach the stomach, ruling out structural abnormalities in the upper digestive tract (data not shown). Fostering *Der2*$^{-/-}$ pups to other lactating dams or removal of their wildtype littermates to decrease competition for food did not increase the survival rate of *Der2*$^{-/-}$ pups (data not shown). We conclude that *Der2*$^{-/-}$ pups die perinatally from a failure to feed, with the rare exceptions described below.

Der2$^{-/-}$ mice show massive perinatal death, yet four percent of *Der2*$^{-/-}$ mice from heterozygous crosses do survive to adulthood. Male *Der2*$^{-/-}$ mice were sterile, despite having normal sperm production as assessed by PAS staining of testes (data not shown). Female *Der2*$^{-/-}$ mice were capable of becoming pregnant, but 3 of 3 pregnancies ended in late-stage abortions requiring euthanasia of the mother. Thus all *Der2*$^{-/-}$ mice studied here were generated by intercrosses of heterozygotes. The few surviving *Der2*$^{-/-}$ mice appeared healthy, although they were consistently smaller than their littermates as measured by body weight (Figure 6C) and skeletal length (*Der2*$^{-/-}$ = 8.9 +/- 0.40 cm; littermates = 9.9 +/- 0.42 cm; $p < 0.00001$). Between 2 and 4 months of age, the surviving *Der2*$^{-/-}$ mice developed a striking involution of the rib cage readily detectable by palpation. This involution became progressively worse with age,

causing hunching and breathing difficulties due to reduced lung volume. Aged *Der2*$^{-/-}$ mice also developed a wasting disease, likely due to their poor overall health status and reduced ability to obtain food. By 12 months of age, all *Der2*$^{-/-}$ mice had to be euthanized.

Skeletons from adult *Der2*$^{-/-}$ mice stained with alizarin red and alcian blue showed normal bone and joint formation with the singular exception of the costal cartilage. *Der2*$^{-/-}$ mice display fusion of the third and fourth sternebrae and develop linear calcifications perpendicular to the axis of rib and periodic nodular thickenings (Figure 6D). To determine when cartilage abnormalities first appeared, skeletal preparations were made from embryonic day 18.5 fetuses. By day 18.5 of gestation, wild type mice showed clear divisions of all sternebrae; however, the third and fourth sternebrae showed slightly delayed separation in *Der2*$^{-/-}$ mice (Figure 6E). No rib abnormalities could be detected in fetal or in one day old *Der2*$^{-/-}$ mice. Thus, defects in cartilage formation are mild at birth and grow progressively worse over time. Given the progressive nature of cartilage defects and the lack of internal hemorrhage in *Der2*$^{-/-}$ pups, we conclude that cartilage defects are unlikely to account for the acute perinatal lethality observed in *Der2*$^{-/-}$ mice. Histological evaluation of adult *Der2*$^{-/-}$ ribs showed a defect in cartilage structure with abnormal chondrocytes (Figure 6F). In addition, many *Der2*$^{-/-}$ chondrocytes contained eosinophilic cytoplasmic inclusions, suggesting a defect in protein secretion or degradation (Figure 6G).

Derlin-2 deficient chondrocytes show intracellular retention of extracellular matrix components.

The skeletal defects in *Der2*$^{-/-}$ mice phenocopy those of a mouse transgenic for mutant collagen oligomeric matrix protein (COMP) (37). COMP mutations in humans lead to either pseudoachondroplasia or multiple epiphyseal dysplasia, diseases marked by short stature and weakened cartilage (38, 39). Secreted COMP normally forms pentamers and, along with collagen IX and matrilin-3, binds to collagen II fibrils. In chondrocytes that express mutant COMP, the intracellularly retained COMP nucleates collagen II fibrils in the ER, causing ER dilation, upregulation of CHOP and ultimately death of the chondrocyte (37). Analysis of *Der2*$^{-/-}$ chondrocytes by electron microscopy likewise revealed ER dilations

consistent with intracellular retention of collagen matrix proteins (Figure 7A and 7B). These ER dilations were observed in *Der2*$^{-/-}$ chondrocytes that had been grown in three-dimensional culture for 1 day or 8 days (Figure 7B). After 18 days of culture, virtually all *Der2*$^{-/-}$ chondrocytes were dead, while wild type chondrocytes were still viable (data not shown). To determine whether ER stress was related to the increase in chondrocyte death, we analyzed expression of CHOP, an apoptosis-inducing protein that is a downstream target of the unfolded protein response. CHOP upregulation was observed in chondrocytes that had been cultured for 8 days (Figure 7C). CHOP transcripts were also upregulated in primary chondrocytes isolated freshly from embryonic day 18.5 *Der2*$^{-/-}$ sternums as well as in cultured chondrocytes (Figure 7D), suggesting an increase in chondrocyte apoptosis in vivo, and not simply a cell culture effect. Both *Der2*$^{-/-}$ and wild type chondrocyte cultures contained collagen fibrils, and no differences in fibril length or diameter were observed by EM (Supplemental Figure 4). Thus, *Der2*$^{-/-}$ chondrocytes are capable of at least some collagen secretion while alive, which is consistent with the mild, progressive nature of the structural abnormalities seen in *Der2*$^{-/-}$ mice. We therefore conclude that skeletal defects observed in *Der2*$^{-/-}$ mice are most likely the result of abnormal ER retention of collagen matrix proteins and a consequent increase in chondrocyte apoptosis.

Discussion

The normal pathways of protein quality control may be compromised either by a reduction in protein folding capability, or by the failure to remove misfolded proteins from the ER. Genetic ablation of ER chaperones is often lethal (3). Genetic deletion of some of the known components of the dislocon would be expected to lead to a blockade in dislocation or to a failure to remove proteins from the ER. The Derlin family of proteins provides an attractive target for such attempts at interference, since they have not been linked to any normal cellular functions other than ER dislocation. We chose to generate a Derlin-2 conditional knockout mouse because Derlin-2 is ubiquitously expressed and is the strongest interacting partner of the ER-resident ubiquitin ligase HRD1/Sel1L.

Der2$^{-/-}$ MEFs show impaired dislocation of the misfolded substrates RI332 and NHK, in accordance with data obtained using a dominant negative version of Derlin-2 and shRNA approaches to knock down expression of *Der2*. *Der2*$^{-/-}$ MEFs showed strong induction of UPR components, implying the accumulation of misfolded proteins in these cells, although we have yet to determine the identity of candidate misfolded proteins in these MEFs. However, the extent to which induction of the UPR is caused by accumulation of misfolded proteins or is engaged by other malfunctions in the ER is not easily ascertained. With the exception of B cells, all *Der2*$^{-/-}$ cell types and tissues examined showed tonic induction of the UPR, with tissue-specific differences in the upregulation of the various components. Known members of the dislocation complex showed compensatory upregulation in *Der2*$^{-/-}$ cells. Sel1L, HRD-1 and Ubc6e levels were elevated in almost every cell type examined. OS-9 levels were higher in *Der2*$^{-/-}$ MEFs and chondrocytes, but showed little expression in hepatocytes or B cells. Derlin-1, which is known to form hetero-oligomeric complexes with Derlin-2 (8), was downregulated in *Der2*$^{-/-}$ cells. Derlin1/2 complexes may form the transmembrane pore through which misfolded substrates traverse the ER bilayer (7, 9). In the absence of Derlin-2, Derlin-1 channels may be less stable, leading to decreased

Derlin-1 protein levels in these cells. In the absence of Derlin-2, misfolded proteins become trapped in the ER and so induce the unfolded protein response.

The physiological consequences of a constitutively active UPR have not been addressed previously. In most tissues, a tonic UPR has no obvious adverse consequences. Cells of the B lymphocyte lineage, including plasma cells which apparently are among the most highly active secretory cells in the body, are unaffected by loss of Derlin-2. Hepatocytes, another highly active secretory cell type, are similarly unaffected by the absence of Derlin-2. *Der2*$^{-/-}$ MEFs survive in tissue culture without overt signs of distress. A tonic increase in expression of proteins associated with dislocation is apparently required by *Der2*$^{-/-}$ cells to thrive. How exactly these upregulated proteins contribute to homeostasis remains to be explored in detail. Contrary to expectations, *Der2*$^{-/-}$ mice are born at Mendelian ratios and die perinatally from a failure to feed. How protein quality control could be related to a failure to feed is currently unclear. Nonetheless, Derlin-2 is not required for survival, since roughly one fifth of the expected *Der2*$^{-/-}$ mice from heterozygous crosses reach adulthood. The few surviving *Der2*$^{-/-}$ mice are normal in most respects, despite having a tonic UPR in all tissues. In fact, the only cells obviously affected by absence of Derlin-2 were costal cartilage chondrocytes. These results illustrate the remarkable homeostatic regulation exerted over protein quality control.

What could cause the observed cartilage defect in *Der2*$^{-/-}$ mice? Chondrocytes express Derlin-2 at a level similar to that seen in most other tissues, and although Derlin-1 levels are reduced in *Der2*$^{-/-}$ chondrocytes, Derlin-1 is not altogether absent. Chondrocytes are highly active secretory cells, but why other cells with an equally high secretory burden should be unaffected by loss of Derlin-2 is not immediately obvious. One possible explanation is that collagen matrix proteins are exquisitely sensitive to errors in protein folding. Knockout mice for COMP or matrilin-3 have virtually no phenotype, yet mice transgenic for point mutations in these same proteins develop skeletal displasias (37, 40-42). Small amounts of misfolded collagen matrix proteins can lead to huge deposits of fibrillar collagen in the ER, and cause decreased collagen secretion, culminating in death of the affected chondrocytes. *Perk*$^{-/-}$ mice

develop skeletal abnormalities due to inadequate secretion of collagen I by osteoblasts, a cell type that expresses unusually high levels of PERK. Dense granules, presumably composed of collagen fibrils, accumulate in the ER of *Perk*$^{-/-}$ osteoblasts (43). Thus we speculate that *Der2*$^{-/-}$ chondrocytes accumulate extracellular matrix proteins in the ER, leading to distension of the ER and death of the affected chondrocytes. The progressive loss of chondrocytes with age would explain the progressive nature of the cartilage defects in *Der2*$^{-/-}$ mice.

To our knowledge, the *Der2*$^{-/-}$ mouse is the first example of a viable mouse uniquely deficient in a component involved in protein dislocation. A Sel1L deficient mouse has been reported which is embryonic lethal around E day 13.5 due to brain and liver abnormalities (44, 45); similarly, loss of HRD-1 results in lethality at E day 13.5 due to failure of hematopoiesis in the fetal liver (46). However the lack of viable pups and the fact that Sel1L plays regulatory role in Notch signaling complicate the use of these models for studying the role of dislocation in a whole organism. Although whole body deletion of Derlin-2 results in perinatal lethality with few animals surviving to adulthood, conditional deletion of Derlin-2 will allow further study of the role of protein dislocation in particular organs or tissues of interest.

Methods

Animals: Derlin-2 floxed animals were generated by conventional gene targeting as illustrated in Supplemental Figure 1. Derlin-2 floxed mice were intercrossed with CD19cre+, Albcre+ or CMVcre+ transgenic mice (Jackson labs) to generate *Der2*^{CD19}, *Der2*^{Alb} and *Der2*$^{-/-}$ mice, respectively. All animals were housed at the Whitehead Institute for Biomedical Research, and were maintained according to guidelines approved by the MIT Committee on Animal Care.

Metabolic labeling and pulse chase experiments: Cells were starved in methionine- and cysteine-free medium containing dialyzed serum for 1 hr, then pulse-labeled for 20 min (unless otherwise indicated) with 250 μCi/ml of [^{35}S]-methionine and [^{35}S]-cysteine (PerkinElmer). At the end of each chase interval, cells were lysed in radioimmunoprecipitation assay buffer containing protease inhibitors. Lysates were then analyzed by immunoprecipitation, SDS-PAGE, and fluorography. Band intensity was determined using a phosphor imager (Fujifilm BAS 2500), and quantitation was done using the MultiGauge software (Fujifilm). HA agarose beads (Roche) or primary antibodies to α1-antitrypsin (Novus Biologicals), MHC class I (p8), IgM (Southern Biotechnology Associates), or Apolipoprotein B (Lifespan Biosciences) combined with Protein G sepharose (Sigma) were used for immunoprecipitations.

Antibodies, reagents and immunoblotting: Cell lysates were prepared using conventional RIPA buffer supplemented with protease inhibitors (Calbiochem). Lysates were clarified at 16,000g for 10 min at 4°C, resolved by SDS-PAGE (10% acrylamide) and electrophoretically transferred onto a nitrocellulose membrane, which was then blocked with 5% non-fat milk in PBS-T (PBS containing 0.05% Tween 20, pH 7.4) before incubation with a primary antibody. After incubating with horseradish peroxidase (HRP)-conjugated secondary antibody (SouthernBiotech), the PBS-T washed membrane was developed using the Western Lightning™ Chemiluminescence Reagent PLUS system (PerkinElmer). The following

commercial antibodies were used for immunoblotting: XBP-1 (Santa Cruz), IRE-1α (Cell Signaling), eIF2α (Cell Signaling), actin (Sigma), calreticulin (Stressgen), p97 (Fitzgerald), OS-9 (Novus Biologicals), HRD-1 (Novus Biologicals), GRP94 (Stressgen), calnexin (Stressgen), α1-antitrypsin (Novus Biologicals), transferrin (Novus Biologicals), MTP (BD), CHOP (Santa Cruz). Antibodies to Derlin-1, Derlin-2, Sel1L, BiP, Ubc6e and PDI were generated in our laboratory.

Flow cytometry: The following antibodies for flow cytometry were obtained from BD Pharmingen: IgM (11/41 or R6-60.2), IgD (11-26c.2a), CD1d (1B1), CD19 (MB19-1), CD23 (B3B4), CD43 (1B11), CD138 (281-2), B220 (RA3-6B2), AA4.1 and GL7. Live B cells were stained with the indicated Abs and analyzed by a FACSCalibur flow cytometer (BD Biosciences). Data were analyzed using CellQuest (BD Biosciences).

Cell culture: Mouse embryonic fibroblasts were prepared by dissection and mechanical disruption of embryonic day 14.5 fetuses obtained from pregnant *Der2*$^{+/-}$ females mated to *Der2*$^{+/-}$ males. Livers and hearts were removed and the remaining carcass pieces were digested overnight in 0.02% trypsin at 4^{o}C. The tissue pellet was then resuspended in DMEM containing 10% fetal calf serum and plated into 10cm tissue culture dishes. Individual embryos were genotyped, and all experiments using wild type and *Der2*$^{-/-}$ MEFs were performed using MEFs derived from the same litter. Naïve B lymphocytes were purified from mouse spleen by magnetic depletion of CD43-positive cells (Miltenyi Biotech). Naïve B cells were cultured in RPMI 1640 media containing 10% FBS with or without LPS (20 μg/ml). Primary hepatocytes were isolated and cultured from *Der2*^{Alb} mice or their cre-negative littermates. Briefly, mice were anesthetized with an intraperitoneal injection of ketamine (87 mg/kg body wt; Webster Veterinary, Sterling, MA, USA) plus xylazine (13 mg/kg body wt; Webster Veterinary). Thereafter, the inferior vena cava was exposed, cannulated, and perfused for 5 min with liver perfusion media (Invitrogen), followed by a 10 min perfusion with liver digestion media (Invitrogen), each having been prewarmed to 37°C. The

digested liver was diced in cold hepatocyte wash media (Invitrogen), passed through an 80 µm nylon mesh (Sefar-America, Depew, NY, USA), and washed an additional three times. Cells were pelleted and resuspended in cold Williams E medium containing 10% FBS, 10^{-7} M dexamethasone, 10 µg/ml insulin, and 5 µg/ml transferrin. Viability was estimated by the trypan blue exclusion, and only preparations with viability in excess of 80% were used for experiments. Cells were plated overnight in 6-well Primaria plates (BD Biosciences, San Jose, CA, USA) at a density of 5×10^5 per well. Chondrocytes were isolated from fetal ribs and sternums that had been digested in 2mg/mL collagenase P (Roche) for 4 hours at 37°C. Chondrocytes were centrifuged in 15 mL tubes and cultured as a three-dimensional pellet in DMEM:F12 supplemented with 10% fetal calf serum.

Glucose, triglyceride, elastase assays: Serum glucose was measured using a One Touch glucose meter. Serum triglycerides were measured using a triglyceride determination kit (Sigma) as per the manufacturer's instructions. Elastase inhibition was performed using diluted serum as indicated and a fixed concentration of porcine elastase in a fluorescence based activity assay (Invitrogen).

Skeletal preparations: Adult or fetal mice were skinned, eviscerated, and fixed in 95% ethanol. Then skeletons were stained by Alizarin red S/Alcian blue and sequentially cleared in 1% potassium hydroxide.

EM analysis: Chondrocytes in either monolayer or 3-D pellet cultures were fixed for electron microscopy after culturing for 14 days to allow for matrix deposition. The cells were fixed in 2.5% glutaraldehyde, 3% paraformaldehyde, with 5% sucrose in 0.1 M sodium cacodylate buffer (pH 7.4). Cells were then postfixed in 1% OsO_4 in veronal-acetate buffer. The cells were stained in block overnight with 0.5% uranyl acetate in veronal-acetate buffer (pH 6.0), dehydrated, and embedded in Spurr's resin. Sections were cut on a Reichert Ultracut E microtome with a Diatome diamond knife at a thickness setting of 50

nm, and stained with 2% uranyl acetate, followed by 0.1% lead citrate. Samples were examined using an FEI Tecnai Spirit TEM at 80 KV and imaged with an AMT camera.

Neuronal imaging: Animals were transcardially perfused with cold phosphate buffered saline followed by 4% paraformaldehyde in 0.1M phosphate buffer. Tissue was postfixed with the same fixative and was washed thoroughly with PB. Neural tissue was dissected free and was cryoprotected by sequential overnight incubations in 15% and 30% w/v sucrose in 0.1M PB. Tissue was embedded in OCT, frozen and cut into 20 micron serial sections on a cryostat. Tissue sections were mounted on slides, and were stained with cresyl violet or were immunostained with a panel of antibodies using methods described in Barnes et al. Cell 2007. SMI312 anti-neurofilament mAb (Covance Research Products) and Alexa-488 conjugated goat anti-mouse secondary antibodies were used to visualize axon tracts. Epifluorescence and transmitted light images were collected from matched sections from different regions of the brains of 2 controls and 2 *Der2*$^{-/-}$.

Quantitative PCR: Chondrocytes were isolated from embryonic day 18.5 mice. RNA was prepared from freshly isolated chondrocytes or from cells that had been cultured for 14 days. RNA extraction was performed using Trizol (Invitrogen), and cDNA was synthesized using Superscript II (Invitrogen). Quantitative PCR was performed using SYBR green and the following primers: actinF AGCACAGCTTCTTTGCAGCTCCTT; actinR CAGCGCAGCGATATCGTCATCCAT; chopF ACAGAGCCAGAATAACAGCCGGAA; chopR TGCTTTCAGGTGTGGTGGTGTATG.

Acknowledgements

SKD is supported by a fellowship from the Cancer Research Institute. HP is supported by grants from the National Institutes of Health.

References

1. Chaudhuri, T.K., and Paul, S. 2006. Protein-misfolding diseases and chaperone-based therapeutic approaches. *Febs J* 273:1331-1349.
2. Loureiro, J., and Ploegh, H.L. 2006. Antigen presentation and the ubiquitin-proteasome system in host-pathogen interactions. *Adv Immunol* 92:225-305.
3. Ni, M., and Lee, A.S. 2007. ER chaperones in mammalian development and human diseases. *FEBS Lett* 581:3641-3651.
4. Molinari, M., Calanca, V., Galli, C., Lucca, P., and Paganetti, P. 2003. Role of EDEM in the release of misfolded glycoproteins from the calnexin cycle. *Science* 299:1397-1400.
5. Mueller, B., Klemm, E.J., Spooner, E., Claessen, J.H., and Ploegh, H.L. 2008. SEL1L nucleates a protein complex required for dislocation of misfolded glycoproteins. *Proc Natl Acad Sci U S A* 105:12325-12330.
6. Mueller, B., Lilley, B.N., and Ploegh, H.L. 2006. SEL1L, the homologue of yeast Hrd3p, is involved in protein dislocation from the mammalian ER. *J Cell Biol* 175:261-270.
7. Lilley, B.N., and Ploegh, H.L. 2004. A membrane protein required for dislocation of misfolded proteins from the ER. *Nature* 429:834-840.
8. Lilley, B.N., and Ploegh, H.L. 2005. Multiprotein complexes that link dislocation, ubiquitination, and extraction of misfolded proteins from the endoplasmic reticulum membrane. *Proc Natl Acad Sci U S A* 102:14296-14301.
9. Ye, Y., Shibata, Y., Yun, C., Ron, D., and Rapoport, T.A. 2004. A membrane protein complex mediates retro-translocation from the ER lumen into the cytosol. *Nature* 429:841-847.
10. Ye, Y., Shibata, Y., Kikkert, M., van Voorden, S., Wiertz, E., and Rapoport, T.A. 2005. Inaugural Article: Recruitment of the p97 ATPase and ubiquitin ligases to the site of retrotranslocation at the endoplasmic reticulum membrane. *Proc Natl Acad Sci U S A* 102:14132-14138.
11. Ernst, R., Mueller, B., Ploegh, H.L., and Schlieker, C. 2009. The otubain YOD1 is a deubiquitinating enzyme that associates with p97 to facilitate protein dislocation from the ER. *Mol Cell* 36:28-38.
12. Todd, D.J., Lee, A.H., and Glimcher, L.H. 2008. The endoplasmic reticulum stress response in immunity and autoimmunity. *Nat Rev Immunol* 8:663-674.
13. Harding, H.P., Zhang, Y., and Ron, D. 1999. Protein translation and folding are coupled by an endoplasmic-reticulum-resident kinase. *Nature* 397:271-274.
14. Lu, P.D., Harding, H.P., and Ron, D. 2004. Translation reinitiation at alternative open reading frames regulates gene expression in an integrated stress response. *J Cell Biol* 167:27-33.
15. Haze, K., Yoshida, H., Yanagi, H., Yura, T., and Mori, K. 1999. Mammalian transcription factor ATF6 is synthesized as a transmembrane protein and activated by proteolysis in response to endoplasmic reticulum stress. *Mol Biol Cell* 10:3787-3799.
16. Bertolotti, A., Zhang, Y., Hendershot, L.M., Harding, H.P., and Ron, D. 2000. Dynamic interaction of BiP and ER stress transducers in the unfolded-protein response. *Nat Cell Biol* 2:326-332.
17. Shamu, C.E., and Walter, P. 1996. Oligomerization and phosphorylation of the Ire1p kinase during intracellular signaling from the endoplasmic reticulum to the nucleus. *Embo J* 15:3028-3039.
18. Calfon, M., Zeng, H., Urano, F., Till, J.H., Hubbard, S.R., Harding, H.P., Clark, S.G., and Ron, D. 2002. IRE1 couples endoplasmic reticulum load to secretory capacity by processing the XBP-1 mRNA. *Nature* 415:92-96.

19. Sriburi, R., Jackowski, S., Mori, K., and Brewer, J.W. 2004. XBP1: a link between the unfolded protein response, lipid biosynthesis, and biogenesis of the endoplasmic reticulum. *J Cell Biol* 167:35-41.
20. Harding, H.P., Zeng, H., Zhang, Y., Jungries, R., Chung, P., Plesken, H., Sabatini, D.D., and Ron, D. 2001. Diabetes mellitus and exocrine pancreatic dysfunction in perk-/- mice reveals a role for translational control in secretory cell survival. *Mol Cell* 7:1153-1163.
21. Wu, J., Rutkowski, D.T., Dubois, M., Swathirajan, J., Saunders, T., Wang, J., Song, B., Yau, G.D., and Kaufman, R.J. 2007. ATF6alpha optimizes long-term endoplasmic reticulum function to protect cells from chronic stress. *Dev Cell* 13:351-364.
22. Yamamoto, K., Sato, T., Matsui, T., Sato, M., Okada, T., Yoshida, H., Harada, A., and Mori, K. 2007. Transcriptional induction of mammalian ER quality control proteins is mediated by single or combined action of ATF6alpha and XBP1. *Dev Cell* 13:365-376.
23. Luo, S., Mao, C., Lee, B., and Lee, A.S. 2006. GRP78/BiP is required for cell proliferation and protecting the inner cell mass from apoptosis during early mouse embryonic development. *Mol Cell Biol* 26:5688-5697.
24. Reimold, A.M., Etkin, A., Clauss, I., Perkins, A., Friend, D.S., Zhang, J., Horton, H.F., Scott, A., Orkin, S.H., Byrne, M.C., et al. 2000. An essential role in liver development for transcription factor XBP-1. *Genes Dev* 14:152-157.
25. Bertolotti, A., Wang, X., Novoa, I., Jungreis, R., Schlessinger, K., Cho, J.H., West, A.B., and Ron, D. 2001. Increased sensitivity to dextran sodium sulfate colitis in IRE1beta-deficient mice. *J Clin Invest* 107:585-593.
26. Kaser, A., Lee, A.H., Franke, A., Glickman, J.N., Zeissig, S., Tilg, H., Nieuwenhuis, E.E., Higgins, D.E., Schreiber, S., Glimcher, L.H., et al. 2008. XBP1 links ER stress to intestinal inflammation and confers genetic risk for human inflammatory bowel disease. *Cell* 134:743-756.
27. Reimold, A.M., Iwakoshi, N.N., Manis, J., Vallabhajosyula, P., Szomolanyi-Tsuda, E., Gravallese, E.M., Friend, D., Grusby, M.J., Alt, F., and Glimcher, L.H. 2001. Plasma cell differentiation requires the transcription factor XBP-1. *Nature* 412:300-307.
28. Hu, C.C., Dougan, S.K., McGehee, A.M., Love, J.C., and Ploegh, H.L. 2009. XBP-1 regulates signal transduction, transcription factors and bone marrow colonization in B cells. *Embo J* 28:1624-1636.
29. McGehee, A.M., Dougan, S.K., Klemm, E.J., Shui, G., Park, B., Kim, Y.M., Watson, N., Wenk, M.R., Ploegh, H.L., and Hu, C.C. 2009. XBP-1-deficient plasmablasts show normal protein folding but altered glycosylation and lipid synthesis. *J Immunol* 183:3690-3699.
30. Adachi, Y., Yamamoto, K., Okada, T., Yoshida, H., Harada, A., and Mori, K. 2008. ATF6 is a transcription factor specializing in the regulation of quality control proteins in the endoplasmic reticulum. *Cell Struct Funct* 33:75-89.
31. Lee, A.H., Iwakoshi, N.N., and Glimcher, L.H. 2003. XBP-1 regulates a subset of endoplasmic reticulum resident chaperone genes in the unfolded protein response. *Mol Cell Biol* 23:7448-7459.
32. Oda, Y., Okada, T., Yoshida, H., Kaufman, R.J., Nagata, K., and Mori, K. 2006. Derlin-2 and Derlin-3 are regulated by the mammalian unfolded protein response and are required for ER-associated degradation. *J Cell Biol* 172:383-393.
33. Zhang, K., Wong, H.N., Song, B., Miller, C.N., Scheuner, D., and Kaufman, R.J. 2005. The unfolded protein response sensor IRE1alpha is required at 2 distinct steps in B cell lymphopoiesis. *J Clin Invest* 115:268-281.
34. Zinszner, H., Kuroda, M., Wang, X., Batchvarova, N., Lightfoot, R.T., Remotti, H., Stevens, J.L., and Ron, D. 1998. CHOP is implicated in programmed cell death in response to impaired function of the endoplasmic reticulum. *Genes Dev* 12:982-995.

35. Zhou, M., Fisher, E.A., and Ginsberg, H.N. 1998. Regulated Co-translational ubiquitination of apolipoprotein B100. A new paradigm for proteasomal degradation of a secretory protein. *J Biol Chem* 273:24649-24653.
36. Fisher, E.A., Lapierre, L.R., Junkins, R.D., and McLeod, R.S. 2008. The AAA-ATPase p97 facilitates degradation of apolipoprotein B by the ubiquitin-proteasome pathway. *J Lipid Res* 49:2149-2160.
37. Schmitz, M., Niehoff, A., Miosge, N., Smyth, N., Paulsson, M., and Zaucke, F. 2008. Transgenic mice expressing D469Delta mutated cartilage oligomeric matrix protein (COMP) show growth plate abnormalities and sternal malformations. *Matrix Biol* 27:67-85.
38. Briggs, M.D., Hoffman, S.M., King, L.M., Olsen, A.S., Mohrenweiser, H., Leroy, J.G., Mortier, G.R., Rimoin, D.L., Lachman, R.S., Gaines, E.S., et al. 1995. Pseudoachondroplasia and multiple epiphyseal dysplasia due to mutations in the cartilage oligomeric matrix protein gene. *Nat Genet* 10:330-336.
39. Hecht, J.T., Nelson, L.D., Crowder, E., Wang, Y., Elder, F.F., Harrison, W.R., Francomano, C.A., Prange, C.K., Lennon, G.G., Deere, M., et al. 1995. Mutations in exon 17B of cartilage oligomeric matrix protein (COMP) cause pseudoachondroplasia. *Nat Genet* 10:325-329.
40. Ko, Y., Kobbe, B., Nicolae, C., Miosge, N., Paulsson, M., Wagener, R., and Aszodi, A. 2004. Matrilin-3 is dispensable for mouse skeletal growth and development. *Mol Cell Biol* 24:1691-1699.
41. Leighton, M.P., Nundlall, S., Starborg, T., Meadows, R.S., Suleman, F., Knowles, L., Wagener, R., Thornton, D.J., Kadler, K.E., Boot-Handford, R.P., et al. 2007. Decreased chondrocyte proliferation and dysregulated apoptosis in the cartilage growth plate are key features of a murine model of epiphyseal dysplasia caused by a matn3 mutation. *Hum Mol Genet* 16:1728-1741.
42. Svensson, L., Aszodi, A., Heinegard, D., Hunziker, E.B., Reinholt, F.P., Fassler, R., and Oldberg, A. 2002. Cartilage oligomeric matrix protein-deficient mice have normal skeletal development. *Mol Cell Biol* 22:4366-4371.
43. Zhang, P., McGrath, B., Li, S., Frank, A., Zambito, F., Reinert, J., Gannon, M., Ma, K., McNaughton, K., and Cavener, D.R. 2002. The PERK eukaryotic initiation factor 2 alpha kinase is required for the development of the skeletal system, postnatal growth, and the function and viability of the pancreas. *Mol Cell Biol* 22:3864-3874.
44. Francisco, A.B., Singh, R., Li, S., Vani, A.K., Yang, L., Munroe, R.J., Diaferia, G., Cardano, M., Biunno, I., Qi, L., et al. Deficiency of suppressor enhancer Lin12 1 like (SEL1L) in mice leads to systemic endoplasmic reticulum stress and embryonic lethality. *J Biol Chem* 285:13694-13703.
45. Li, S., Francisco, A.B., Munroe, R.J., Schimenti, J.C., and Long, Q. SEL1L deficiency impairs growth and differentiation of pancreatic epithelial cells. *BMC Dev Biol* 10:19.
46. Yagishita, N., Ohneda, K., Amano, T., Yamasaki, S., Sugiura, A., Tsuchimochi, K., Shin, H., Kawahara, K., Ohneda, O., Ohta, T., et al. 2005. Essential role of synoviolin in embryogenesis. *J Biol Chem* 280:7909-7916.

Table 1

B cell subset	Markers	control	Der2CD19
Marginal zone B cells	CD19+CD21hiCD23loCD1d+	9.0 +/- 4.2	8.7 +/- 4.7
Follicular B cells	CD19+CD21+CD23+	61.7 +/- 2.7	60.6 +/- 3.5
Transitional (T1)	CD23loAA4.4+	12.0 +/- 5.6	10.7 +/- 4.4
Transitional (T2)	CD23+AA4.1+	10.6 +/- 6.3	8.4 +/- 3.7
Germinal center B cells	CD19+GL7+	5.6 +/- 2.6	4.2 +/- 1.5
IgM+IgDlo spleen cells	IgM+IgDlo	21.5 +/- 4.8	21.2 +/- 5.0
IgM+IgD+ spleen cells	IgM+IgD+	30.6 +/- 10.3	31.8 +/- 6.0
IgMloIgD+ spleen cells	IgMloIgD+	33.7 +/- 11.3	29.3 +/- 5.7
CD138+ B220+ spleen cells	CD138+B220+	3.1 +/- 1.2	2.0 +/- 1.0
CD138+ B220lo spleen cells	CD138+B220lo	1.5 +/- 0.8	1.1 +/- 0.6
Pro B cells	B220+CD43+CD19lo	4.9	5.8 +/- 0.4
Pre B cells	B220+CD43+CD19+	24.2	18.4 +/- 2.2
Bone marrow plasma cells	CD138+B220+	19.5 +/- 1.1	20.1 +/- 4.1
Peritoneal cavity B-1 cells	CD19+B220lo	11.4 +/- 8.5	25.6 +/- 10.5

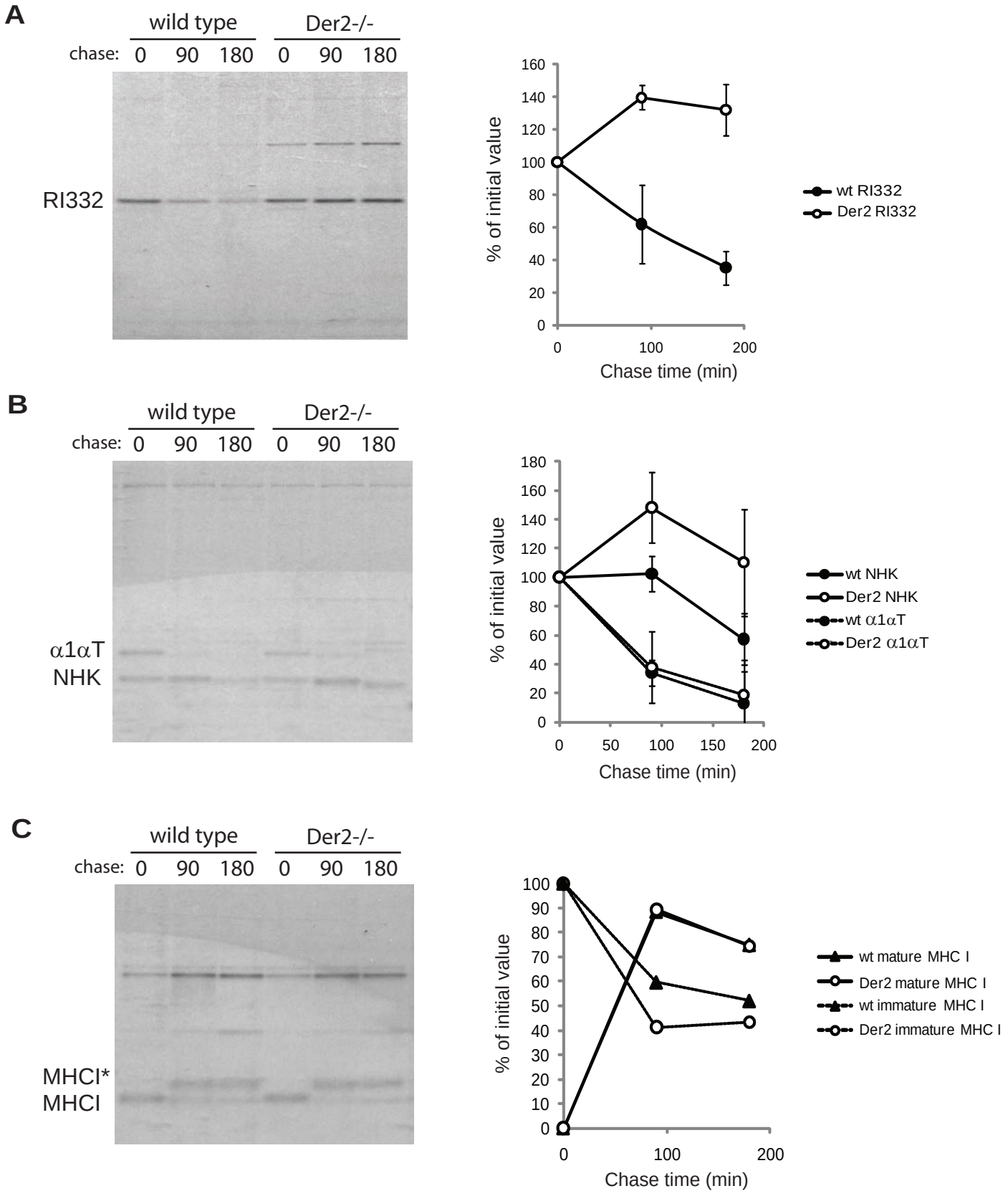

Figure 1: *Der2*$^{-/-}$ MEFs show impaired protein dislocation. A) RI332-HA transfected MEFs were starved for one hour, pulsed with ^{35}S cysteine and methionine for 20 minutes, and chased in non-radioactive media for the indicated times. Cells were lysed in NP-40 lysis buffer and immunoprecipitated with anti-HA beads. Samples were analyzed by SDS-PAGE, and band intensity was quantified using a phosphoimager. A representative gel is shown on the left. Quantification of three independent experiments is shown on the right. B) MEFs were transfected with α1-antitrypsin (α1αT) and Null Hong Kong (NHK) plasmids and subjected to pulse-chase analysis as in A. Lysates were immunoprecipitated with an antibody to α1-antitrypsin. A representative gel is shown on the left. Quantification of three independent experiments is shown on the right. C) MEFs were subjected to pulse-chase analysis as in (A). Lysates were immunoprecipitated with anti-MHC I antiserum.

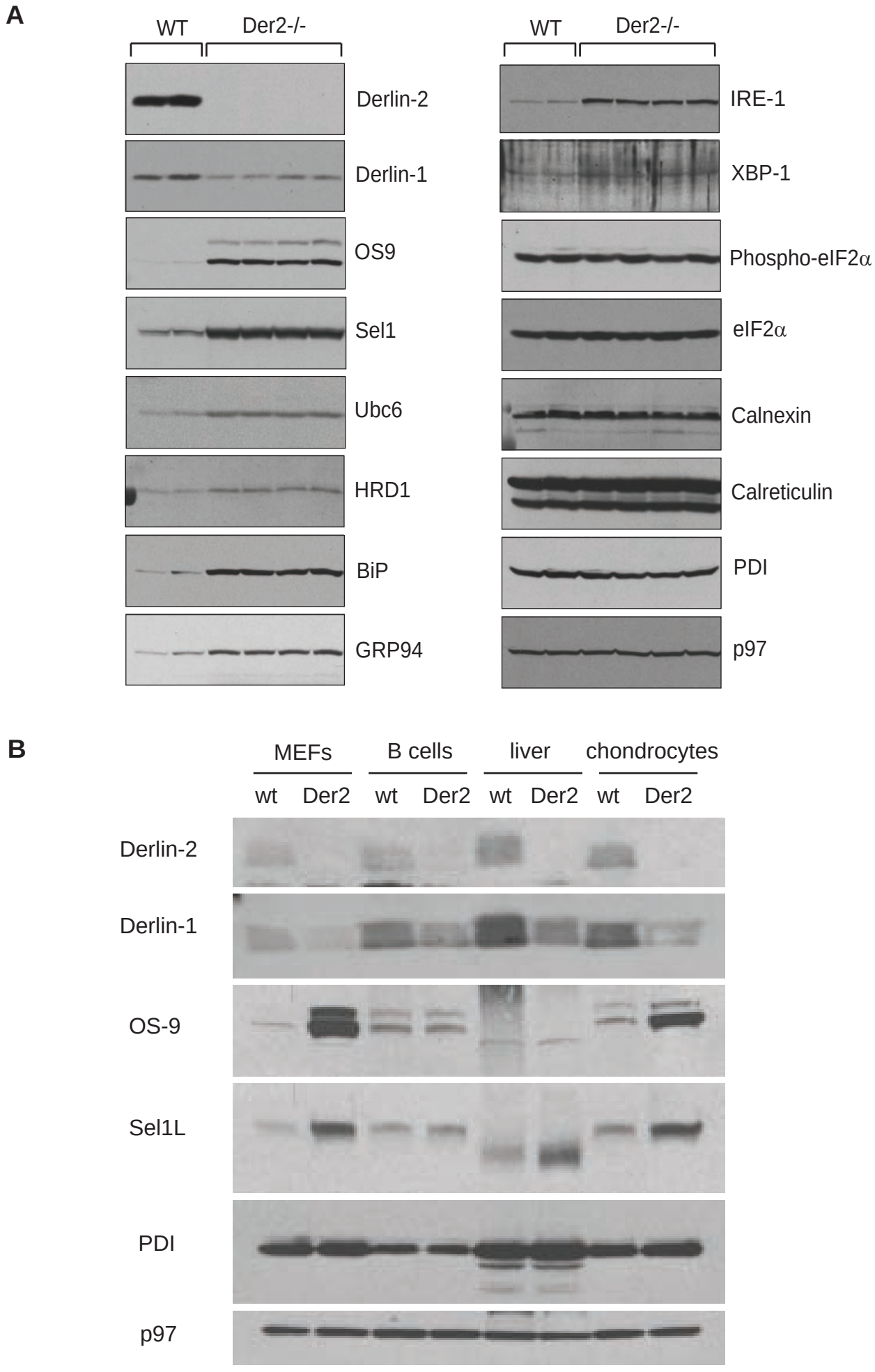

Figure 2: *Der2*$^{-/-}$ cells upregulate members of the dislocation complex and show a constitutive unfolded protein response. A) NP-40 lysates from two wild type and four *Der2*$^{-/-}$ lines of MEFs were immunoblotted using the indicated antibodies. B) NP-40 lysates were prepared from MEFs, naïve B cells, freshly isolated hepatocytes, or chondrocytes. Lysates were normalized for total protein content, subjected to SDS PAGE, and immunoblotted using the indicated antibodies.

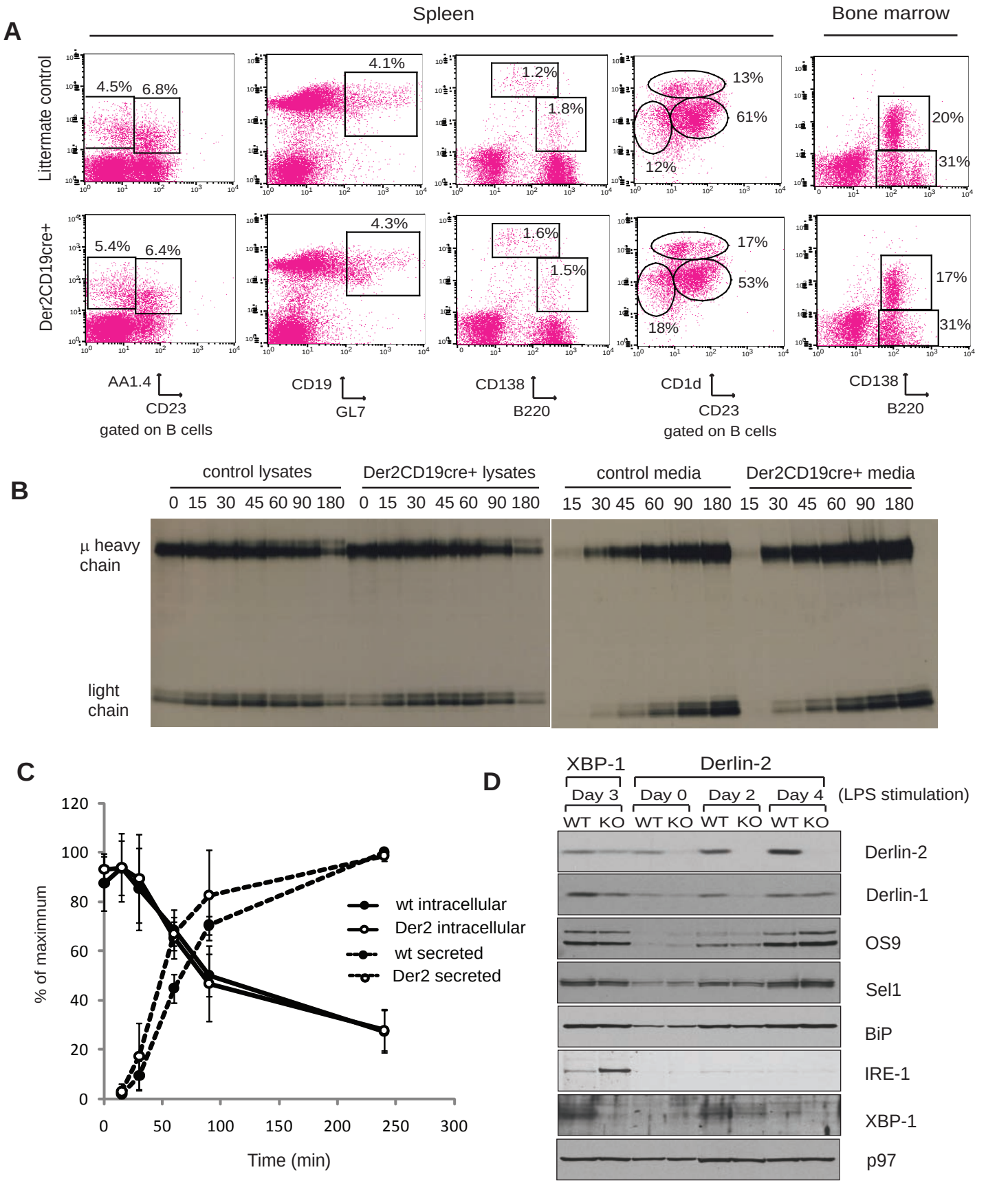

Figure 3: Derlin-2 deficiency has no effect on B cells. A) Spleen and bone marrow cells were harvested from *Der2*^{CD19} mice or their cre-negative littermates. B cell subsets were analyzed by flow cytometry. One representative mouse is shown for each genotype; means for multiple mice are shown in Table 1. B) B cells were isolated from *Der2*^{CD19} mice or their cre-negative littermates and cultured for 3 days in media with LPS. Cells were then cultured in cysteine and methionine-free media for one hour, pulsed with ^{35}S cysteine and methionine for 10 minutes, and chased in non-radioactive media for the indicated times. Cells were lysed in NP-40 lysis buffer, immunoprecipitated using anti-IgM antiserum, and analyzed by SDS-PAGE. C) Quantification of three independent experiments performed as in (B). D) B cells were harvested from wild type, *Xbp1*^{CD19}, or *Der2*^{CD19} mice and cultured in media containing LPS for the indicated number of days. Cells were lysed in NP-40 lysis buffer, subjected to SDS-PAGE, and immunoblotted using the indicated antibodies.

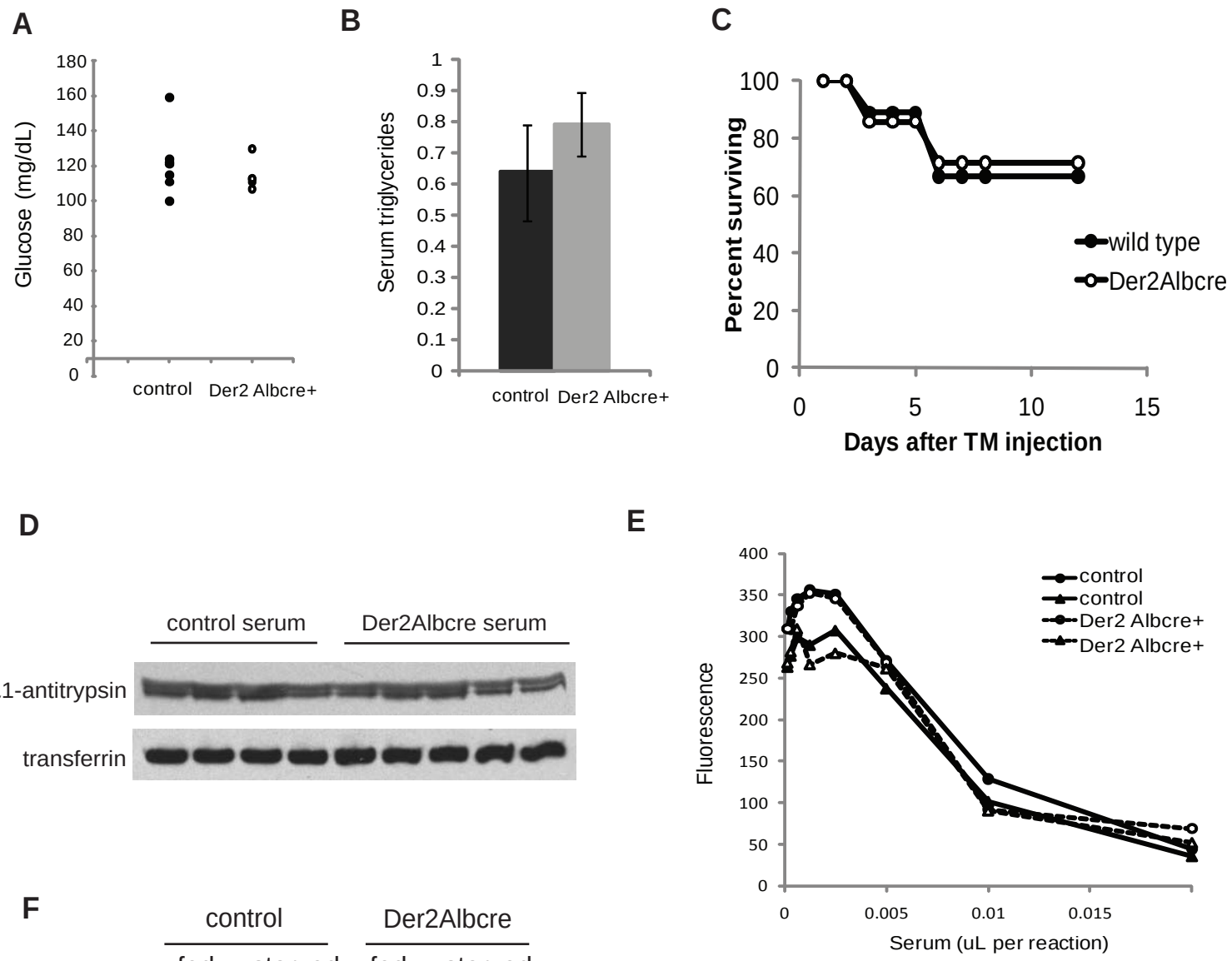

Figure 4: Derlin-2 deficiency has no effect on liver function. A) Adult *Der2*^{Alb} mice or their cre-negative littermates were fasted overnight and blood glucose levels were measured using a glucose monitoring system. B) Adult *Der2*^{Alb} mice or their cre-negative littermates were fasted overnight and serum triglycerides were measured. C) *Der2*^{Alb} mice or their cre-negative littermates were injected intraperitoneally with tunicamycin (1 mg/kg) and body weight was monitored over time. Mice were euthanized when they reached 80% of initial body weight. D) Serum from *Der2*^{Alb} mice or their cre-negative littermates was subjected to SDS-PAGE and immunoblotted using the indicated antibodies. E) Serum from two *Der2*^{Alb} mice and two littermate controls was added to an elastase activity assay to determine the relative levels of inhibitory serum anti-serine proteases. F) *Der2*^{Alb} mice or their cre-negative littermates were fasted or not fasted for 24 hours. Livers were perfused with PBS, harvested and lysed in NP-40 lysis buffer. Lysates were subjected to SDS-PAGE and immunoblotted using the indicated antibodies.

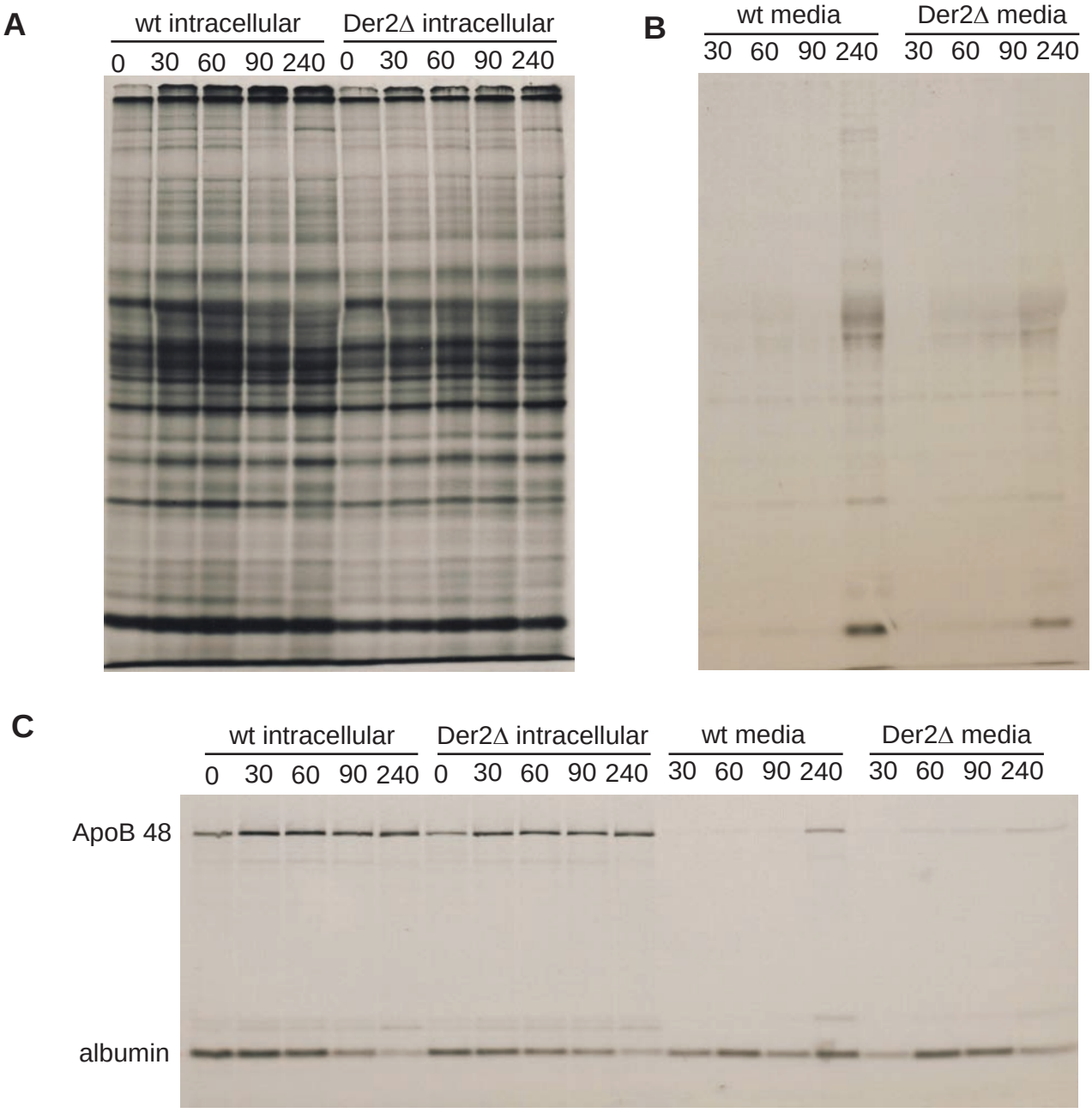

Figure 5: Derlin-2 deficiency has no effect on protein synthesis in isolated hepatocytes. A) Hepatocytes were isolated from *Der2*^{Alb} mice or their cre-negative littermates. Cells were cultured in cysteine and methionine-free media for one hour, pulsed with ^{35}S cysteine and methionine for 20 minutes, and chased in non-radioactive media for the indicated times. Cells were lysed in NP-40 lysis buffer, and whole lysates were subjected to SDS-PAGE. B) Hepatocytes were treated as in (A) and media fractions were collected at each time point to assess secreted proteins. Equal volumes of media were subjected to SDS-PAGE. C) Hepatocytes treated as in (A) were lysed in NP-40 lysis buffer. Lysates were immunoprecipitated using anti-apolipoprotein B antiserum, and samples were subjected to SDS-PAGE. D) Quantification of (C).

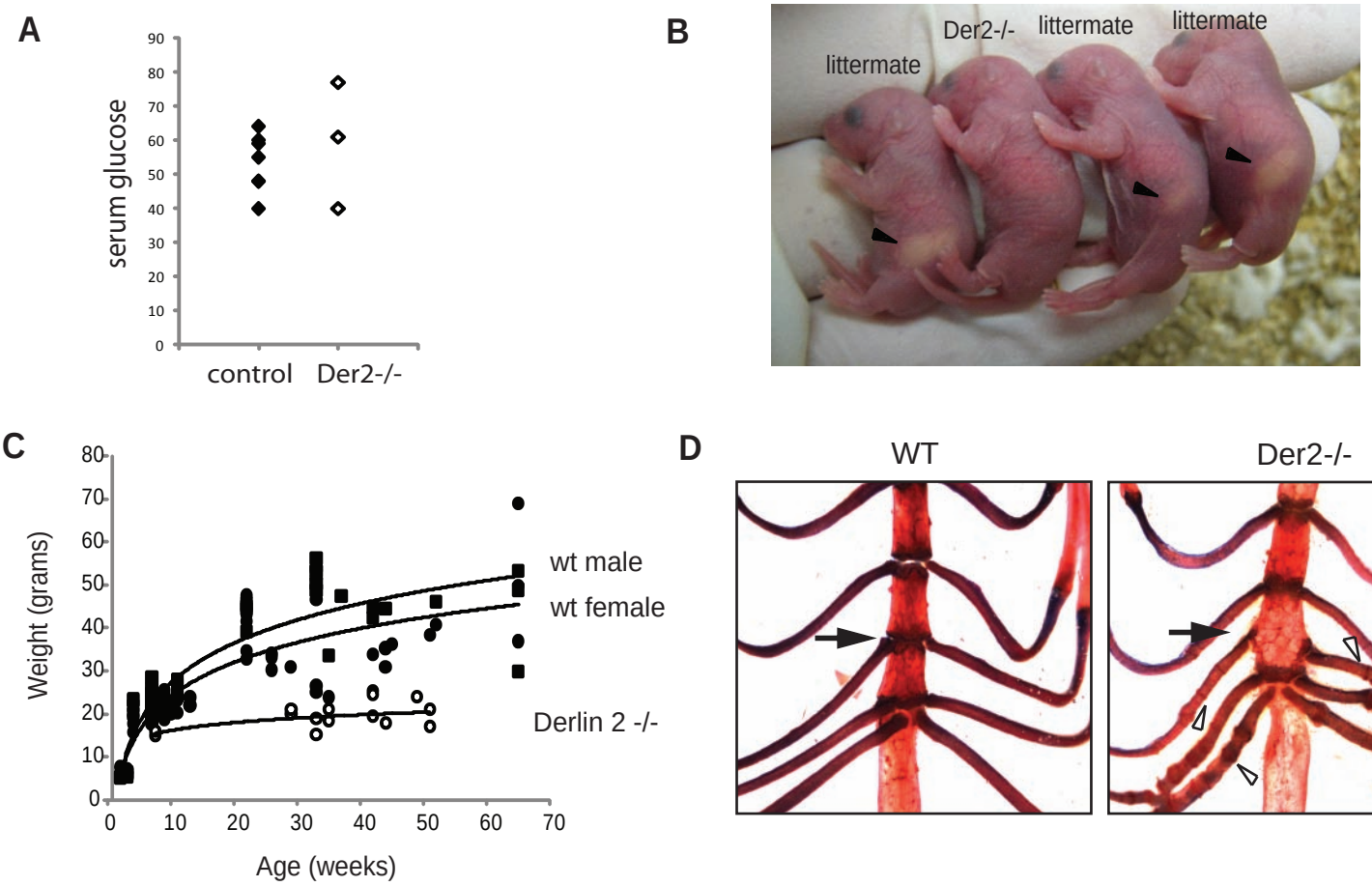

Figure 6: Whole body deletion of Derlin-2 leads to perinatal lethality and cartilage defects. A) A litter containing *Der2*$^{-/-}$ pups was delivered via caesarean section and not permitted to feed for two hours. Serum glucose levels were measured. B) One day old pups from a litter containing a *Der2*$^{-/-}$ mouse. Milk spots indicated by arrowheads. C) Body weights of *Der2*$^{-/-}$ mice and littermate controls at various ages. *Der2*$^{-/-}$ mice did not survive beyond 52 weeks. *Der2*$^{-/-}$ male and female mice did not vary significantly in their weights. D) Skeletons of a nine-month old *Der2*$^{-/-}$ and wild type control mouse were harvested and stained with Alizarin red and Alcian blue. Note the bottom three pairs of ribs connect to a single sternebrae in the *Der2*$^{-/-}$ mouse, indicating fusion of the 3rd and 4th sternebrae (arrow). *Der2*$^{-/-}$ rib cartilage is punctuated with linear calcifications (open arrowheads). E) Skeletons were harvested from E day 18.5 *Der2*$^{-/-}$ and wild type embryos and stained with Alizarin red and Alcian blue. Note the ossification center (arrow) between the 3rd and 4th sternebrae is smaller in *Der2*$^{-/-}$ mice. F) Hematoxylin and eosin staining of rib cartilage from adult mice (20x magnification). G) Sections were prepared as in (F). Arrows indicate chondrocytes with eosinophilic cytoplasmic inclusions in adult *Der2*$^{-/-}$ mice.

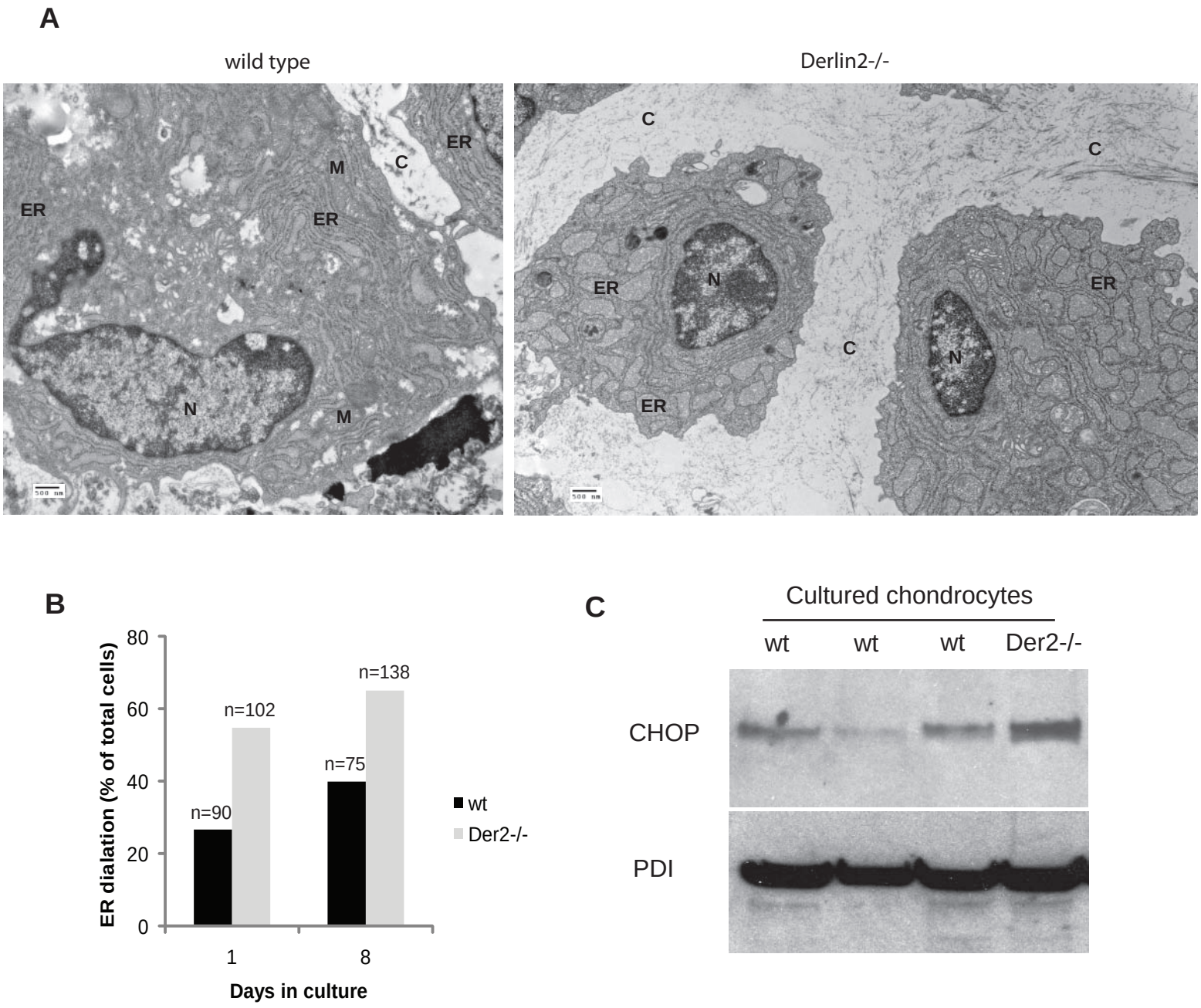

Figure 7: *Der2*$^{-/-}$ chondrocytes show intracellular retention of extracellular matrix proteins. A) Chondrocytes were isolated from wild type or *Der2*$^{-/-}$ embryonic day 18.5 mice were maintained in 3D pellet culture for 8 days prior to fixation, sectioning and analysis by EM. Both samples contained similar amounts of extracellular collagen fibrils. Note the distended ER in *Der2*$^{-/-}$ chondrocytes. N, nucleus; M, mitochondrion; C, collagen fibers. B) Chondrocytes were cultured as in (A) for 1 day or 8 days. Cells were analyzed by electron microscopy and scored as dilated or not dilated. Total number of cells (n) counted per group is indicated above each bar. C) Protein lysates were harvested from chondrocytes that had been cultured for 8 days. Lysates were analyzed by SDS-PAGE and immunoblotted using the indicated antibodies. Note the increased CHOP expression in *Der2*$^{-/-}$ chondrocytes. D) RNA was isolated from freshly isolated embryonic day 18.5 chondrocytes or chondrocytes that had been maintained in culture for 2 weeks, and cDNA was prepared. Quantitative PCR was performed using primers specific for *Chop* and normalized to β-*actin*. *, $p<0.005$.

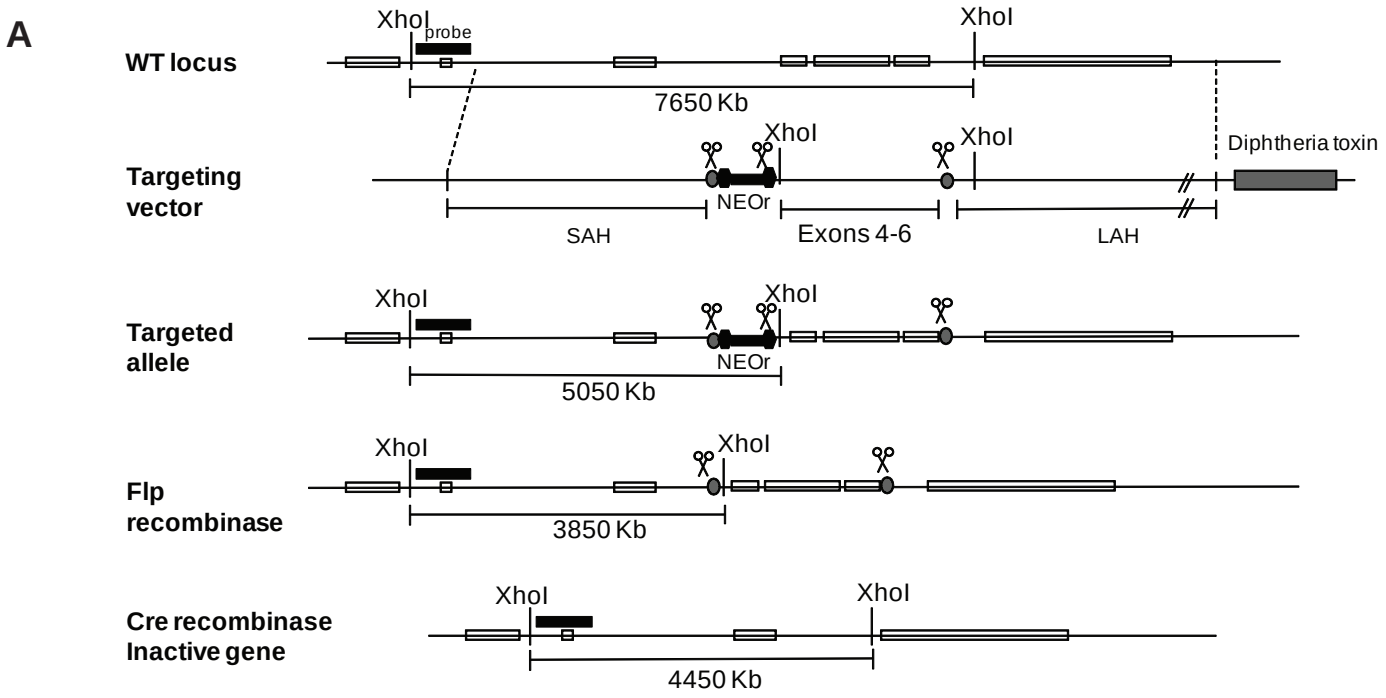

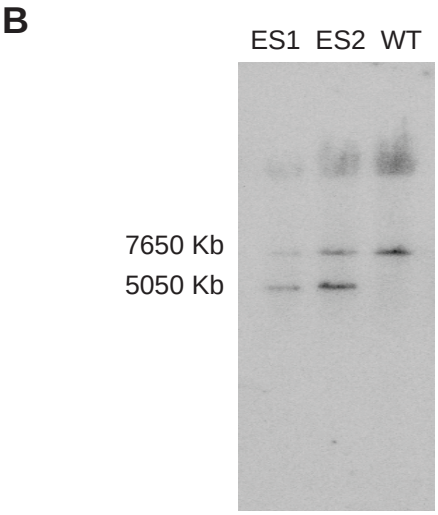

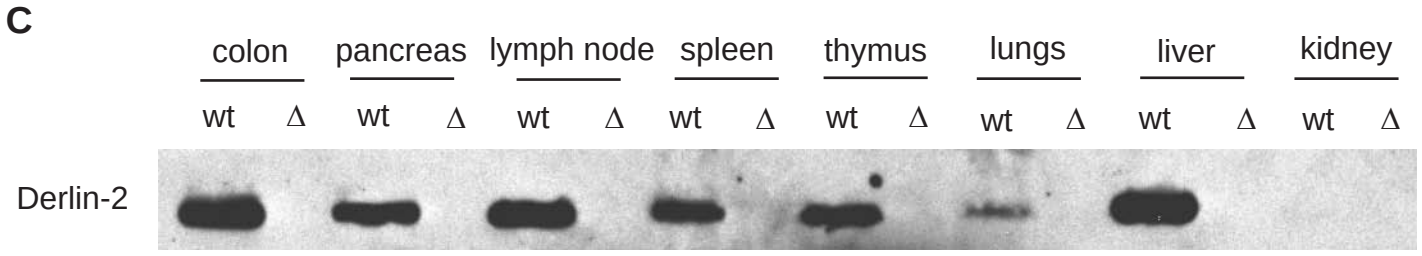

Supplemental Figure 1: Generation of Derlin-2 floxed mouse. A) Schematic diagram of the Derlin-2 genomic locus, targeting construct and genomic locus of the resulting *Der2*$^{-/-}$ mouse after cre-mediated deletion. B) Genomic DNA was prepared from two lines of targeted ES cells or control ES cells and Southern blotted using the probe indicated in (A). Correct targeting of the Derlin-2 locus is indicated by the presence of a 5050 Kb band. C) NP-40 lysates were prepared from the indicated tissues of a *Der2*$^{-/-}$ mouse or littermate control. Samples were subjected to SDS-PAGE and immunoblotted for Derlin-2.

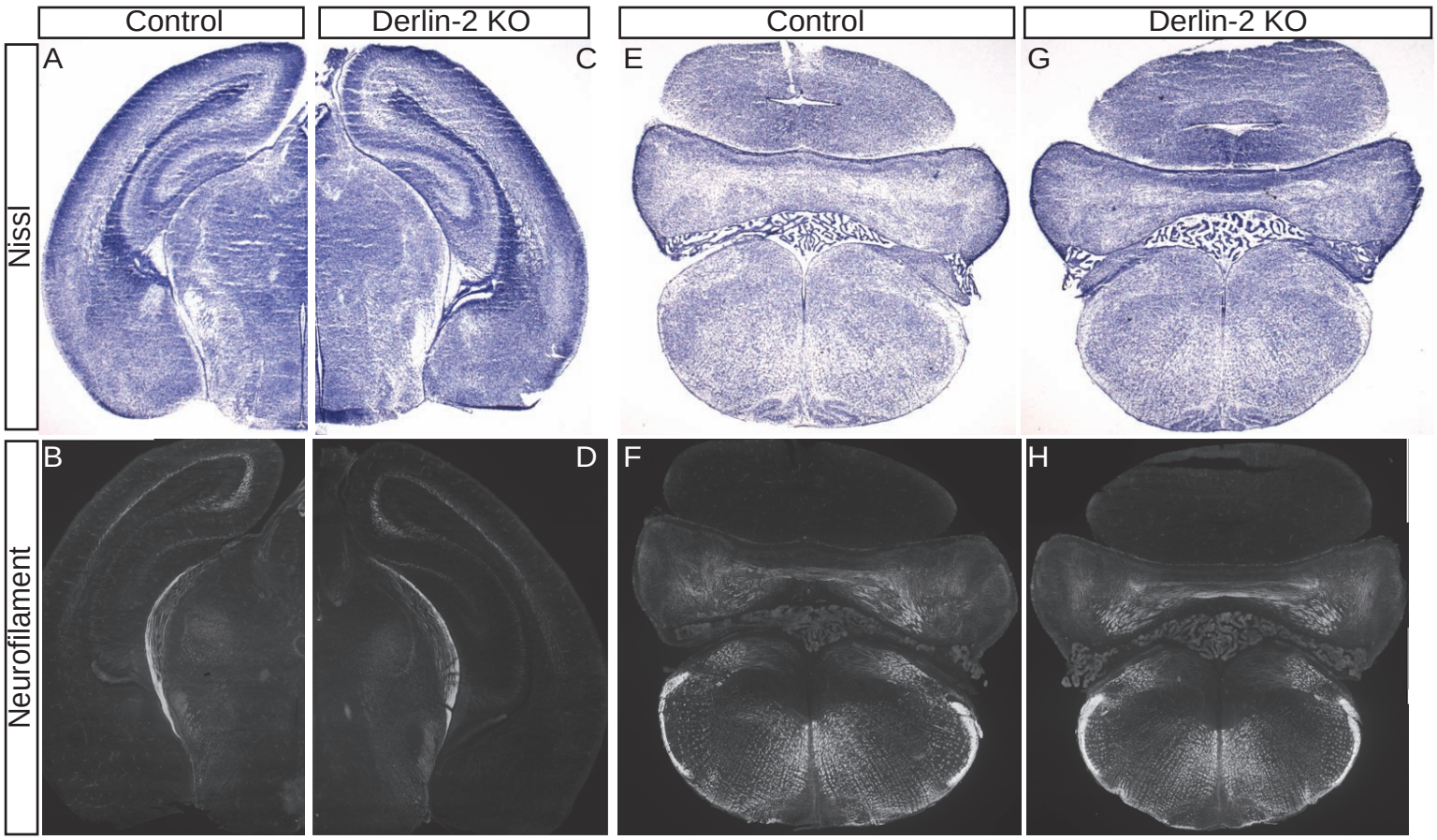

Supplemental Figure 2: Nissl and neurofilament staining demonstrate that major axon tracts and the gross structure of the brain are intact at postnatal day 0 in the *Der2*$^{-/-}$ (C,D,G,H) as compared to a littermate control (A,B,E,F). Serial sections from the level of the optic tract (A-D) or from Spinal trigeminal nucleus interpolaris (E-H) were stained as indicated. Immunostaining for activated caspase-3 revealed no evidence of increased apoptosis in the central nervous system of *Der2*$^{-/-}$ animals (not shown). Peripheral nerves and spinal ganglia were also not grossly affected by the loss of Derlin-2. Phrenic innervation of the diaphragm was normal as were the appearance of neuromuscular junctions as determined by whole mount immunohistochemistry of diaphragm muscle (data not shown).

Wild type

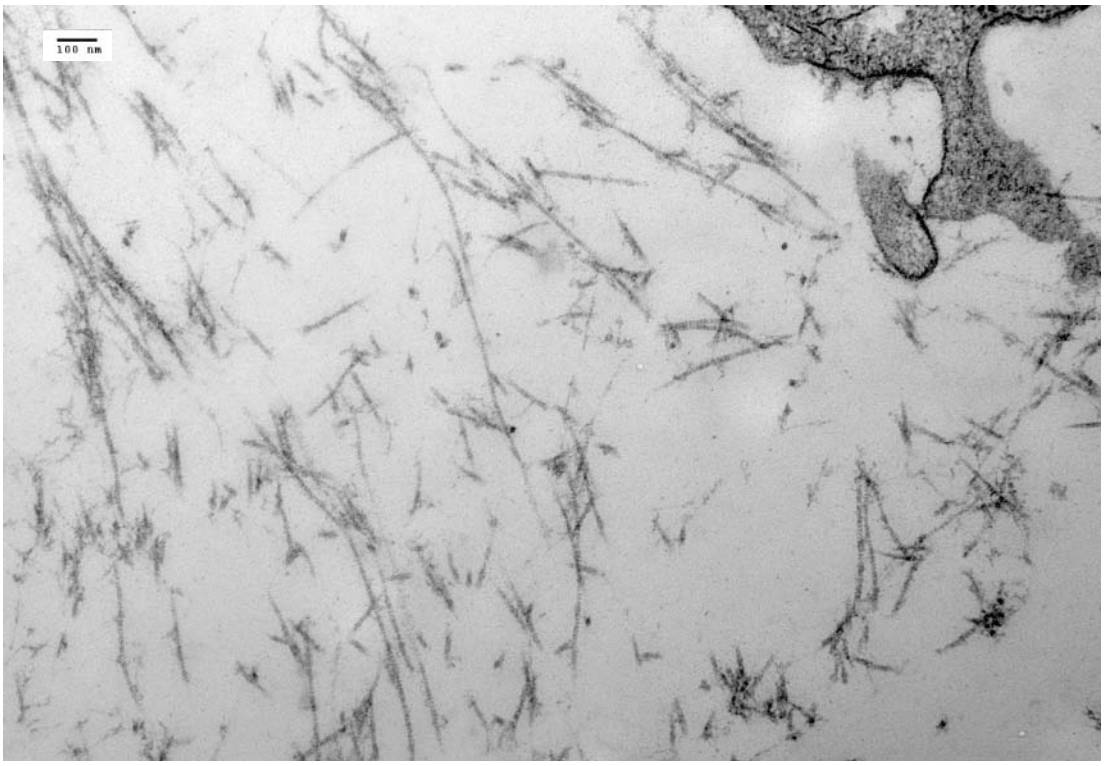

Der2-/-

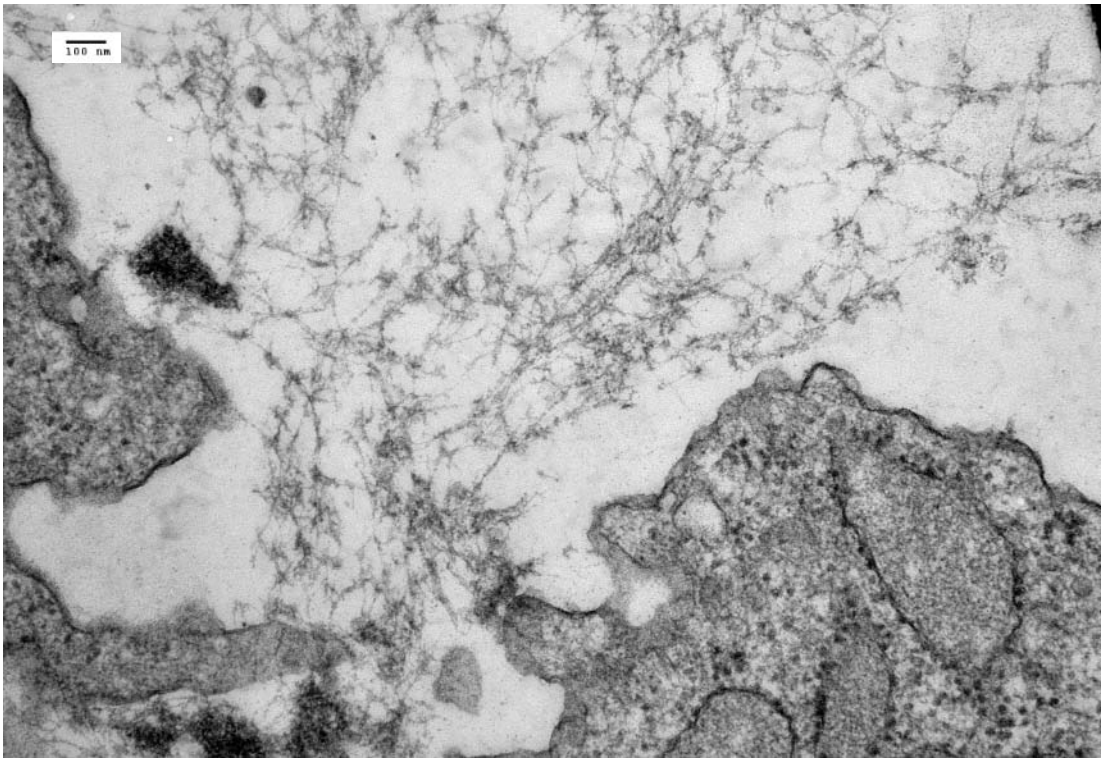

Supplemental Figure 3: Chondrocytes from wild type or *Der2*$^{-/-}$ embryonic day 18.5 mice were maintained in three dimensional culture for 8 days and analyzed by electron microscopy. Shown are collagen fibrils secreted into the extracellular matrix (49,000x magnification).